Draft version September 12, 2023
Typeset using LaTeX **twocolumn** style in AASTeX631

Steadiness of coronal heating

P. Judge[1]

[1] *High Altitude Observatory, National Center for Atmospheric Research, Boulder CO 80307-3000, USA*

(Dated: Accepted . Received ; in original form)

ABSTRACT

The EUI instrument on the Solar Orbiter spacecraft has obtained the most stable, high-resolution images of the solar corona from its orbit with a perihelion near 0.4 AU. A sequence of 360 images obtained at 17.1 nm, between 25-Oct-2022 19:00 and 19:30 UT is scrutinized. One image pixel corresponds to 148 km at the solar surface. The widely-held belief that the outer atmosphere of the Sun is in a continuous state of magnetic turmoil is pitted against the EUI data. The observed plasma variations appear to fall into two classes. By far the dominant behavior is a very low amplitude variation in brightness (1%) in the coronal loops, with larger variations in some footpoint regions. No hints of observable changes in magnetic topology are associated with such small variations. The larger amplitude, more rapid, rarer and less-well organized changes are associated with flux emergence. It is suggested therefore that while magnetic reconnection drives the latter, most of the active corona is heated with no evidence of a role for large-scale (observable) reconnection. Since most coronal emission line widths are subsonic, the bulk of coronal heating, if driven by reconnection, can only be of tangentially discontinuous magnetic fields, with angles below about $0.5 c_S/c_A \sim 0.3\beta$, with β the plasma beta parameter (~ 0.01), and c_S and c_A sound and Alfvén speeds. If heated by multiple small flare-like events, then these must be $\lesssim 10^{21}$ erg, i.e. pico-flares. But processes other than reconnection have yet to be ruled out, such as viscous dissipation, which may contribute to the steady heating of coronal loops over active regions.

Keywords: Solar corona

1. INTRODUCTION

The solar corona is commonly perceived to be in a state of continual dynamic evolution, as it responds to evolving magnetic fields emerging from the physical surface and the more tenuous chromosphere. Several years ago, of four central characteristics deemed important in a review of coronal heating, we read De Moortel & Browning (2015)

> "coronal heating is intrinsically non-steady."

This statement is not debated here. Indeed, theoretical considerations imply that almost all mechanisms must be non-steady on scales of dissipation, which probably lie between ion viscous damping and kinetic scales (100 km to 10 m, e.g. Davila 1994). These mechanisms occur below observational scales currently achieved. But, to what degree does our observational evidence require that the corona be intrinsically variable? Observationally, dynamics is manifested in direct motions resolved in images, and through line profiles revealing unresolved motions. The latter have consistently revealed that the dominant unresolved dynamics is weak, subsonic (Billings 1965; Bray et al. 1984; Thomas & Neupert 1994; Hara & Ichimoto 1999; Raju et al. 2001; Singh et al. 2002; Kosugi et al. 2007; Coyner & Davila 2011; Krishna Prasad et al. 2013; Brooks & Warren 2016; Koutchmy et al. 2019) with very occasional rapid motions associated with observable changes in apparent topology, i.e. magnetic reconnection. But what about observations of resolved motions?

The modern view that the coronal is heated impulsively and dynamically has become so widespread as to be rarely questioned. Of many papers the recent work of Tiwari et al. (2023) is an example in which non-steady coronal behavior is actively sought. One clear excep-

Corresponding author: P. Judge

tion is found in a review, "The dynamic solar corona in X-rays with Yohkoh" by Tsuneta (1996):

> "... Yohkoh observations also show the existence of steadily heated plasmas with temperature of 2 - 4 MK, both in active regions and in the quiet Sun. The mechanism of the steady heating has not yet been understood."

In a related and prescient aticle, (Sturrock 1999) questioned whether the observable magnetic fields are active or passive in heating the corona. He reasoned that coronal heating may well result from processes well below the scales of our observations, i.e. there may be "hidden variables" in the coronal heating problem. This idea appears to be untested, as yet. Indeed, influential studies have sought direct relationships between some measurable magnetic field and coronal heating, with mixed success (Fisher et al. 1998; Mandrini et al. 2000; Aschwanden 2001). It is unclear if the inconclusive results result from Sturrock's idea or if we simply have used data inadequate for purpose.

In viewing recent high-quality movies of Auchère et al. (2023) from the Solar Orbiter EUI instrument (Marsch et al. 2005; Marsden et al. 2013; Rochus et al. 2020, 2022), the present author was struck that the dominant signal from the corona appeared to be constant. A brief inspection of the EUI data suggested also that observed variations appear to be attributable to benign, generally sub-sonic field-aligned flows, which are not necessarily associated with irreversible energy dissipation. At the small scales sampled by EUI (148 km) during these observations, the only clear, rapid "activity" usually associated with magnetic reconnection seemed to be associated with visibly emerging magnetic flux.

The consequences of a dominant mode of apparent steadiness in the brightness of the bulk of coronal loops are intriguing, perhaps even vital to identifying the dominant heating mechanisms. Reconnection, often associated with coronal heating (e.g. Pontin & Priest 2022), appears to be absent most of the time in the data examined here, *on observable scales.*

This paper re-examines the concept that the corona is observed to be in a state of continual dynamic readjustment. This idea has historically been inferred from decades of space observations at X-ray, EUV and UV wavelengths, using evidence that is, when scrutinized, largely indirect (e.g. Viall et al. 2021). Is the observable variability of coronal plasma related directly to irreversible heating, such as commonly assumed by, for example, nanoflares, reconnection or wave turbulence? Or is heating associated with physical processes which are unresolved in space and time? To investigate this question, the primary data used below are a time series of 360 stabilized images at 17.1 nm from the Solar Orbiter EUI instrument obtained over half an hour on 25th October 2022.

2. A BRIEF REVIEW OF CORONAL DYNAMICS AND HEATING

Many articles have derived quantities related to coronal dynamics, under the general picture that the corona observed at X-ray and EUV wavelengths consists of plasma loops. Section 2 of the review by Viall et al. (2021) summarizes the literature on observational constraints on coronal heating, representing perhaps the generally accepted state of the subject.

Following Rosner et al. (1978), the current paradigm within which most studies lie, is that the radiating coronal plasmas represent bundles of "one-dimensional atmospheres" owing to the high conductivity of coronal plasma, the enormous physical scales involved, and the frozen-field condition (Alfvén's theorem, Alfvén 1942). One example of this kind of motion in coronal plasma is described by Peres (2000). In an example of confronting data with theory, Section 4 of Schmelz & Winebarger (2015) analyzed lifetimes of active region plasma loops in terms of necessarily simplified models within the accepted paradigm. Lifetimes were found to be significantly longer than those expected based on the calculated cooling times. This example reveals recurring general problems in such data-model comparisons. In order to make any progress the model simplifications necessarily include a host of assumptions which are justified neither by consideration of first principles, nor by interpretations of available data which are highly non-unique.

In a different approach, based upon some early hard X-ray observations (Lin et al. 1984) and a conflict between the plasma equations of motion and a fixed topology, Parker (1988) proposed that bursts of nanoflares might heat the active corona. In Parker's approach, basic theoretical results in highly conducting plasmas were combined with available observations to propose that flares smaller than those reported by Lin and colleagues may naturally supply a mechanism to deliver ordered magnetic energy into heat via the formation of elementary current sheets (Low 2023). Parker's approach has survived intense scrutiny and prompted a significant community to seek signatures of nanoflares (e.g. Bogachev et al. 2020). Nanoflares have therefore been accepted as a likely candidate to explain heating of long-lived coronal structures (e.g. Pontin & Priest 2022). However, the observational methods used to test the picture have, as above, contain elements which are arguably

Table 1. EUI observations of the corona on 25th October 2022

Times	19:00:00.202	19:29:55.205
Format	2048 × 2048	
Distance to Sun	60,755,600 km	0.406125 A.U.
Number of frames	360	
Cadence	5 seconds	
Pixel size	0.492″	148 km
Bandpass	17.1 nm	

ad-hoc, and details of any "models" are so incomplete to make solid, testable predictions far from our capabilities. In short, this dynamic model remains almost untested by available methods,

A recent monograph by Judge & Ionson (2023) digs deeper into assessing this current understanding. They highlighted many arguments why the current paradigm from basic theory should be re-examined, from basic theory to the limitations of remotely sensed data. It is in this spirit that the current paper asks, using the unique capabilities offered by new capabilities, if, and by how much, the corona is heated steadily. Readers will perhaps be surprised that this question is being asked in 2023, given the general tone within the current literature. For those we ask for patience as the novel data are examined below.

3. OBSERVATIONS

We have analyzed the sequence of images documented in Table 1. The only processing performed beyond the publicly released EUI data was to perform an accurate co-alignment of the time series. All images were aligned to the time-averaged image using cross-correlations. A new average was computed and the process repeated once. The residual jitter is less than 1 pixel (≡ 148 km at the solar surface). These data are comparable to the highest resolution EUV images obtained, with the HiC suborbital rocket experiment (Rachmeler et al. 2022). HiC obtained images at 17.1 nm with a plate scale of 0.129″, which is about 94 km, compared with 148 km in Table 1. The spatial resolution of HiC data assessed by Rachmeler et al. (2022) is complicated by time-dependent jitter, instrument PSF and other properties of the images obtained. The authors concluded that only a fraction of their 5 minutes of data was unaffected by jitter, yielding a resolution > 2× the pixel size or worse. The shorter duration of the sequence of HiC images are less suitable for our explicit goal of studying dynamic evolution of the coronal plasma.

Most of the data analyzed by Rachmeler et al. (2022) achieved widths (FWHM) across coronal strands 0.4″or greater (290 km), essentially the same physical size as the Nyqvist-limited sampling resolution of the EUI images. While these different datasets have similar imaging performance, the Orbiter data span a longer time period. Significantly, the 30 minutes of data is longer than the typical cooling time of coronal loops in active regions of a few minutes.

Figure 1 shows the field-of-view and close-ups. The two bottom panels highlight the same region separated by 60 seconds, to emphasize the two different types of behavior of concern to the present work. "Constant" long coronal loops don't change perceptibly between these two panels. But a region of more broken-up emission evolves more dramatically on short timescales. It would be difficult to identify field-aligned motions in the latter structure, seen "underneath" the more obvious static loops.

A third type of morphological structure is shown in Figure 2, an area of quieter Sun from these same images which is closer to the solar equator. This area shows few, if any, clear loop structures. The diffuse emission does vary on timescales of 60 seconds, but the morphology of the structures is not as clear as those highlighted in Figure 1. The active region data analyzed here are sufficient to address an important aspect of the main question of the nature of coronal heating. The quiet regions will yield different outcomes, but the magnetic lines of force cannot arguable be traced, presenting a challenge to assigning variations as field-aligned or otherwise.

3.1. *Statistics*

Figure 3 shows the simplest possible statistic of variation, i.e. those independently calculated for each of the 2048^2 pixels. The figure shows just the central (most active) part of the EUI field-of-view, to highlight coronal loops. This area lies between those shown in the upper panels of Figure 1.

For each pixel we evaluated the variance $\sigma_{\rm I}^2$ from the time series. The image of $\sigma_{\rm I}$ results almost entirely from solar, not instrumental changes. As noted above, this image is very different from an image of $\sqrt{I_{\rm mean}}$, which is similar to the image of $I_{\rm mean}$ itself.

Aside from several, rare "hot spots" of activity (examples are circled in Fig. 3), the variations as measured merely by $\sigma_{\rm I}/I_{\rm mean}$ lie mostly below 0.1 in the logarithm. The distribution of these variations is shown in the bottom right figure. Above this value, which corresponds to $\sigma_{\rm I}/I_{\rm mean} \geq 10^{0.1} = 0.26$, less than 1% of the pixels show larger variations, The vast bulk of the variations lie near $10^{-1.3} I_{\rm mean}$. The most likely variation in the time series thus corresponds to

$$\sigma_{\rm I} = 0.05 I_{\rm mean}.$$

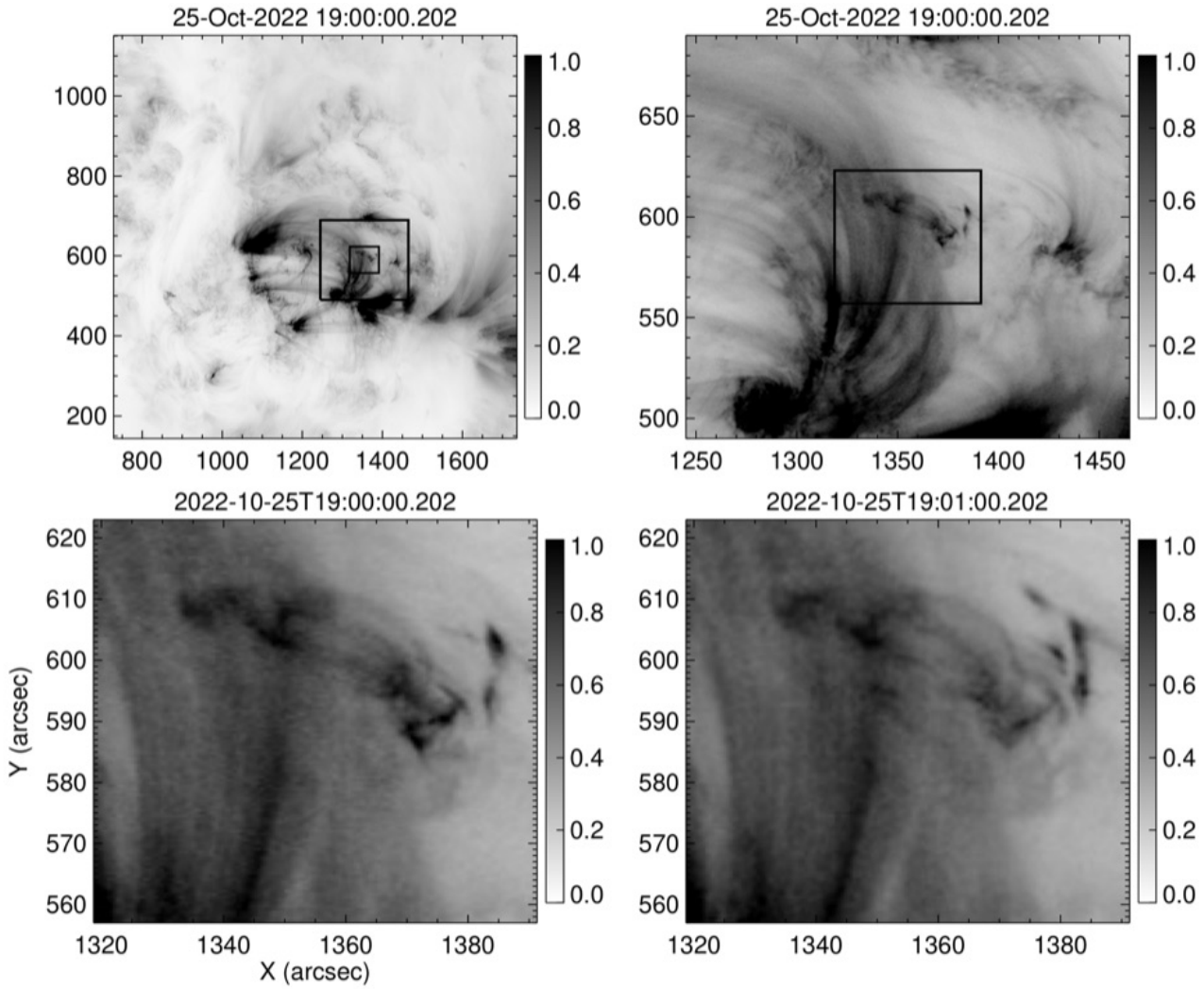

Figure 1. The region of the Sun observed by the EUI instrument is shown as a full field-of-view (top left) and three close-up views. The lower two panels show the two types of structure discussed in this paper, they are separated by just 60 seconds. The large loops are almost unchanged in 60 seconds. However, there is a region of dynamic evolution of EUV brightness in the upper half of these two lower panels, possibly resulting from changes in magnetic topology. Intensities are on an arbitrary but identical scale for all panels. The squares show the areas shown in the right and bottom panels.

The large loop system in the figure has $\sigma_I/I_{\rm mean} \sim 0.01 - 0.02$, which may be a lower limit if coronal motions such as sub-pixel oscillations on the plane of the sky reduce variances. The more highly variable regions marked in red are spatially associated with the circled nests of activity. Figure 4 shows variances split over various frequency ranges. Although these figures show just local behavior, it is clear that there is a great deal of pixel-to-pixel structure in these quantities. Notice in particular the large loop systems in $I_{\rm mean}$ and their unusually small variances along the bulk of the loop lengths. When loop-like variances are larger, they trace out loci which are along plasma loops observed only in the intensity images. Occam's Razor would suggest the interpretation that field-aligned mass, momentum and energy transport, and/or transverse loop oscillations must be responsible for this observation. There is no obvious need to suggest other sources of variation, but this might be explored in future (section 5).

In stark contrast, the smaller-scale nests of large variances are clearly seen as amorphous shapes. Two examples are circled in Figure 3. The nests appear to be examples of a "geyser" phenomenon (Paraschiv & Donea 2019, A. Paraschiv private communication 2023).

Figure 4 shows power in ranges from 0.5-3 mHz, 3-50 mHz, and 50-100 mHz. The only structures with power over all frequencies are associated with the nest near $X = 1365, Y = 605$, which we examine next.

3.2. *Signatures of emerging magnetic flux*

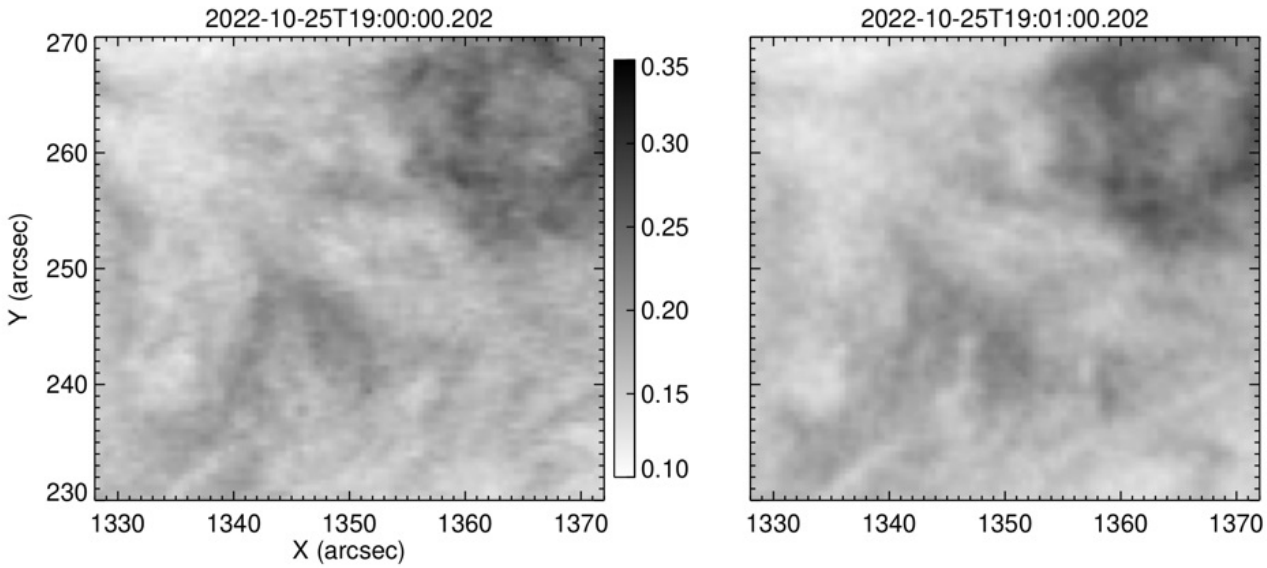

Figure 2. Close-ups of a region of quiet Sun are shown for the same frames shown in Figure 1.

Contemporaneous data from both the HMI and AIA instruments on SDO were examined. Examples are shown in Figure 5, over which the two encircled regions of Solar Orbiter coronal data of Figure 3 are also indicated. Both show emergence of flux of opposite polarity. The larger circled region at $X = -160, Y = 255$ in SDO coordinates emerged $\approx 5 \cdot 10^{19}$ Mx of opposite polarity flux over 2 hours from 15:00 UT. This is typical for this size of emerging region, as observed with HMI (Norton et al. 2017). The other (near $X = -220, Y = 220$) has significantly less emergence of flux of opposite-sign to the dominant polarity. Its behavior typifies other regions nearby.

We might use the images of variances in Figure 3 to identify coronal structures. The first and most obvious is that the loops are readily apparent in images of $\sigma_{\rm I}$, especially near the footpoints (marked with arrows later in Figure 5). The amplitudes of the loops visible in $\sigma_{\rm I}/I_{\rm mean}$ in Figure 3 are almost all below 0.25. Strikingly, the longest loops in the top left of each panel show particularly small variances below 0.05 in $\sigma_{\rm I}/I_{\rm mean}$. The bright coronal structure near $X = 1400, Y = 500$ has variances which are similarly suppressed. Lastly, those structures with the largest variances are geometrically far smaller than the typical active region loops.

The SDO data shown in Figure 5 highlight the central part of the field of view observed by EUI on Solar Orbiter. The plasma loops observed at 1 MK (at 17.1 nm wavelengths) sparsely connect regions marked with arrows The hotter plasma at 9.4 nm (mostly from Fe XVIII formed near 6 MK) is more diffuse. With the co-spatial 13.1 nm emission formed near 0.5 MK, it is clear that this loop system contains a broad distribution of plasma with respect to electron temperature. The bipolar emerging flux region identified by the black circle, exhibits smaller, less smooth coronal structures with increasing temperatures, the opposite of the observed loops.

4. DISCUSSION

This work addresses a very simple question: what does the apparent stability of coronal structure tell us about underlying plasma heating mechanisms? With the advent of excellent data from the EUI instrument of Solar Orbiter, the analysis is accordingly very simple, and as such, stands in contrast to some of the vast literature on related work, which is considerably more complicated, and laden with many more assumptions Viall et al. (see the recent review of 2021). Nevertheless, the present work suggests that significant information has been overlooked for decades. Sometimes in nature it is those data which do not immediately attract our attention which are most important. In this particular case emphasis is given to the *lack* of activity in particular within typical coronal loops in active regions. It was concluded above that the vast bulk of solar coronal plasma over active regions is heated quiescently, when observed on scales down to 150 km. The radically different behavior at 17.1 nm emission between coronal loops and regions of emerging flux has been quantified in various figures. Most notably, the power spectra are heavily weighted towards low frequencies (0-3 mHz) in loops, higher frequencies above emergent regions (Figures 3 and 4). Further, the amplitudes of variation are clearly reduced along larger, long-lived loop systems (see the upper half of the lower

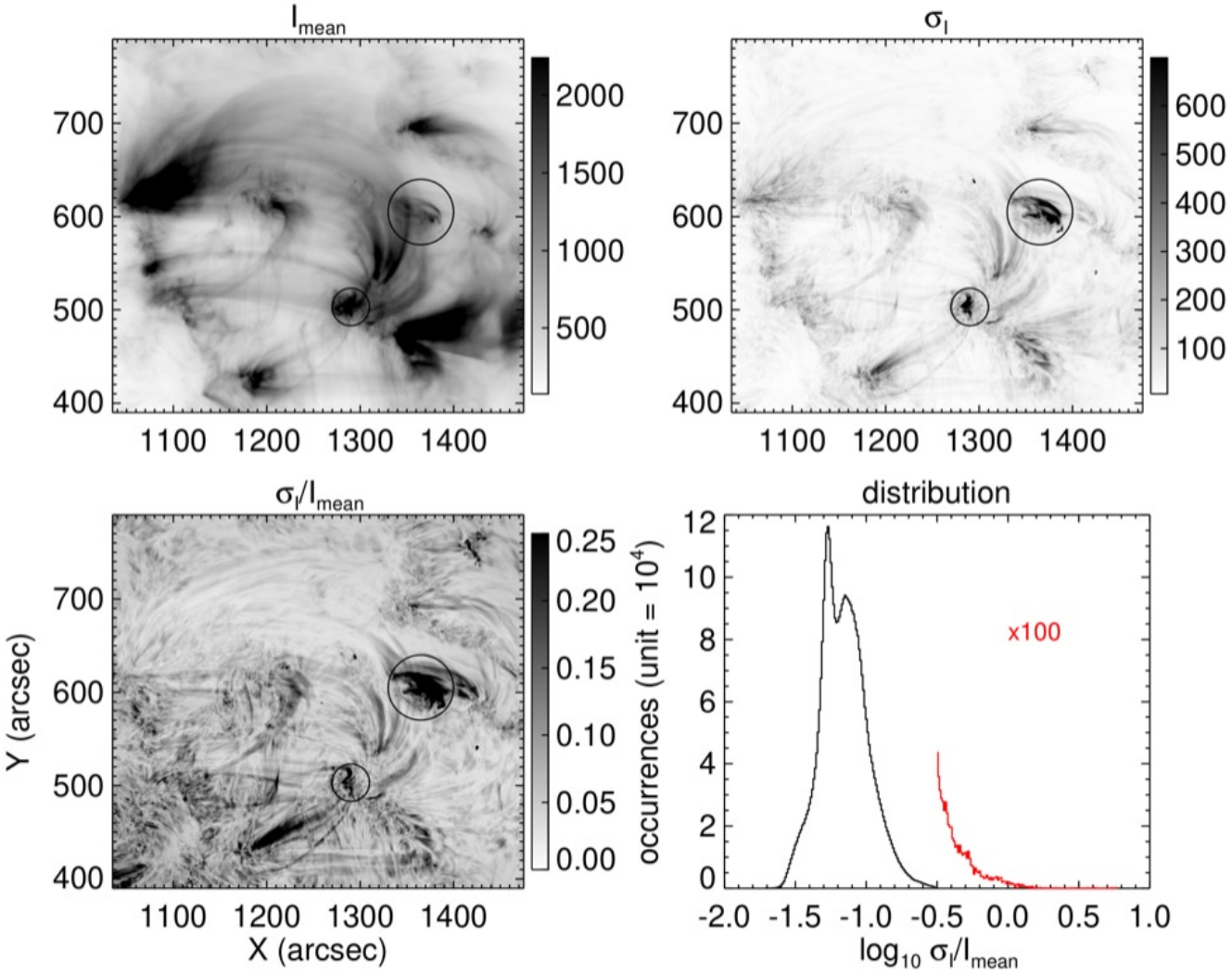

Figure 3. The mean of the timeseries is shown (top left) with the rms variations (top right), and their ratio (bottom left). The encircled region of enhanced variances is also indicated in Figure 5. The line plot shows the distribution of $\log_{10}\sigma_{\rm I}/I_{\rm mean}$, with the occurrences of larger variances magnified by a factor of 100 (red line). Only 0.14% of all the pixels have values of $\log_{10}\sigma_{\rm I}/I_{\rm mean}$ exceeding 0.1 in the logarithm, i.e. with values of $\sigma_{\rm I}$ exceeding the mean by 26%.

left panel of Figure 3). Also, variances are larger in some regions close to loop footpoints, but not all.

4.1. *Possible implications*

Whatever the dominant mode of coronal heating of plasmas near and above 1 MK, it must respect the new basic observational constraints presented here, and the well-documented subsonic coronal emission line widths and shifts. In such conditions, the only significant irreversible fluid effects are energy losses by radiation and an increase of entropy by field-aligned heat conduction, but with no genuine source of irreversible heating, such as shocks. Those near-footpoint regions showing a larger variance than the looptops would appear to correspond to such motions, given the literature on the dynamics of loop footpoints (again one can find a discussion in Viall et al. 2021). In spite of the emphasis on supersonic motions with speeds > 100 km s^{-1} in the literature (e.g. de Pontieu et al. 2009; Raouafi et al. 2023), such motions appear largely absent in some typical active region loops, the vast majority of the time.

If irreversible heating cannot occur through shocks, it must be through another kind of dissipative structure, associated with electrodynamics, hydrodynamic processes having no further avenue for dissipation. Reconnection produces flow speeds of order the Alfvén speed of the oppositely oriented components of the magnetic field. With magnetic field strengths of order $B \sim 100$ G and number densities of protons close to $5 \cdot 10^9$ cm^{-3} for active region loops, the Alfvén speed $c_{\rm A}$ is ~ 2800 km s^{-1}. The linewidths therefore suggest that reconnec-

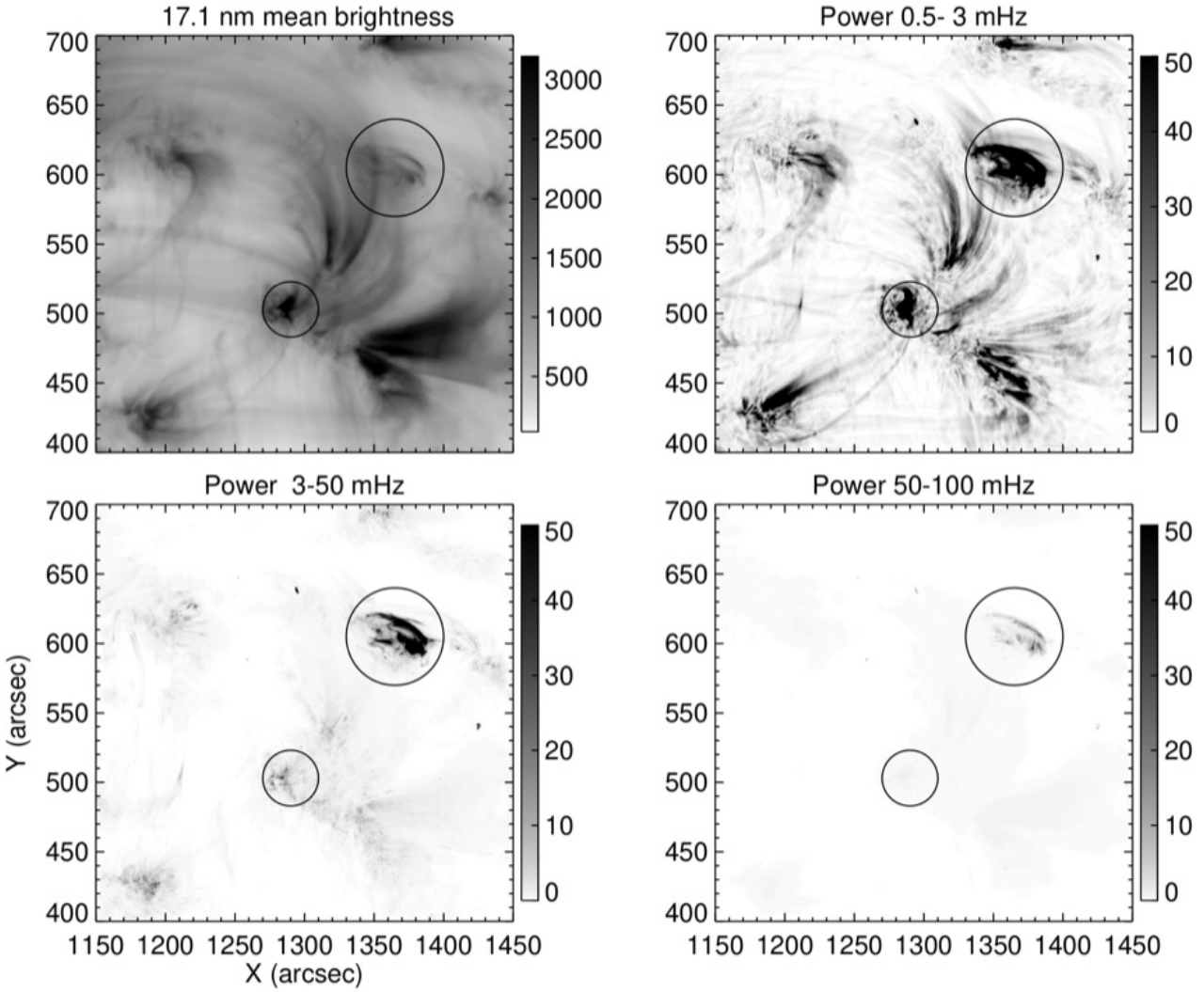

Figure 4. Frequency-delimited variances (integrated power spectra) of the EUI timeseries are shown as in Figure 3.

tion, if important, must involve tangential components of the magnetic field with a strength ≤ 1 G, accompanied by flows of ≤ 30 km s^{-1}. In other words, only tiny fractions of the total magnetic field in the corona must be responsible for coronal heating. Interestingly, Sturrock (1999) already wondered if the measurable magnetic fields defining the coronal topology play an active or passive role in coronal heating.

It is widely recognized that viable heating mechanisms intrinsically involve departures from the symmetry implied in a 1-dimensional picture, even if the fluid is required to flow within such structures (e.g. De Moortel & Browning 2015). In the presence of asymmetries within what appear to be one-dimensional plasma loops, dissipative structures develop through spontaneous current sheet formation, and intermittent phase mixing, resonant absorption, and of internal surface waves. These processes dissipate the ordered energy of velocity gradients, manifested in bulk flows of ions and electrons and differential flows (electric currents), through particle collisions, the final step in irreversible plasma heating. These particular processes are familiarly called viscous and Joule energy dissipation respectively. These sources of heat are absent in flows which are essentially one-dimensional, within strong fields which are close to potential, with weakly compressive motions (e.g. Hollweg 1986). In this regard, on resolvable scales, active regions are frequently surprisingly close to potential fields (Wiegelmann & Sakurai 2021). This appears to be true for the longer loops showing small variances analyzed here (Schrijver et al. 2005).

4.2. *On the role of magnetic reconnection*

Let us examine the hypothesis that coronal loops are heated by processes originating from magnetic reconnection. The word *originating* is important, for there

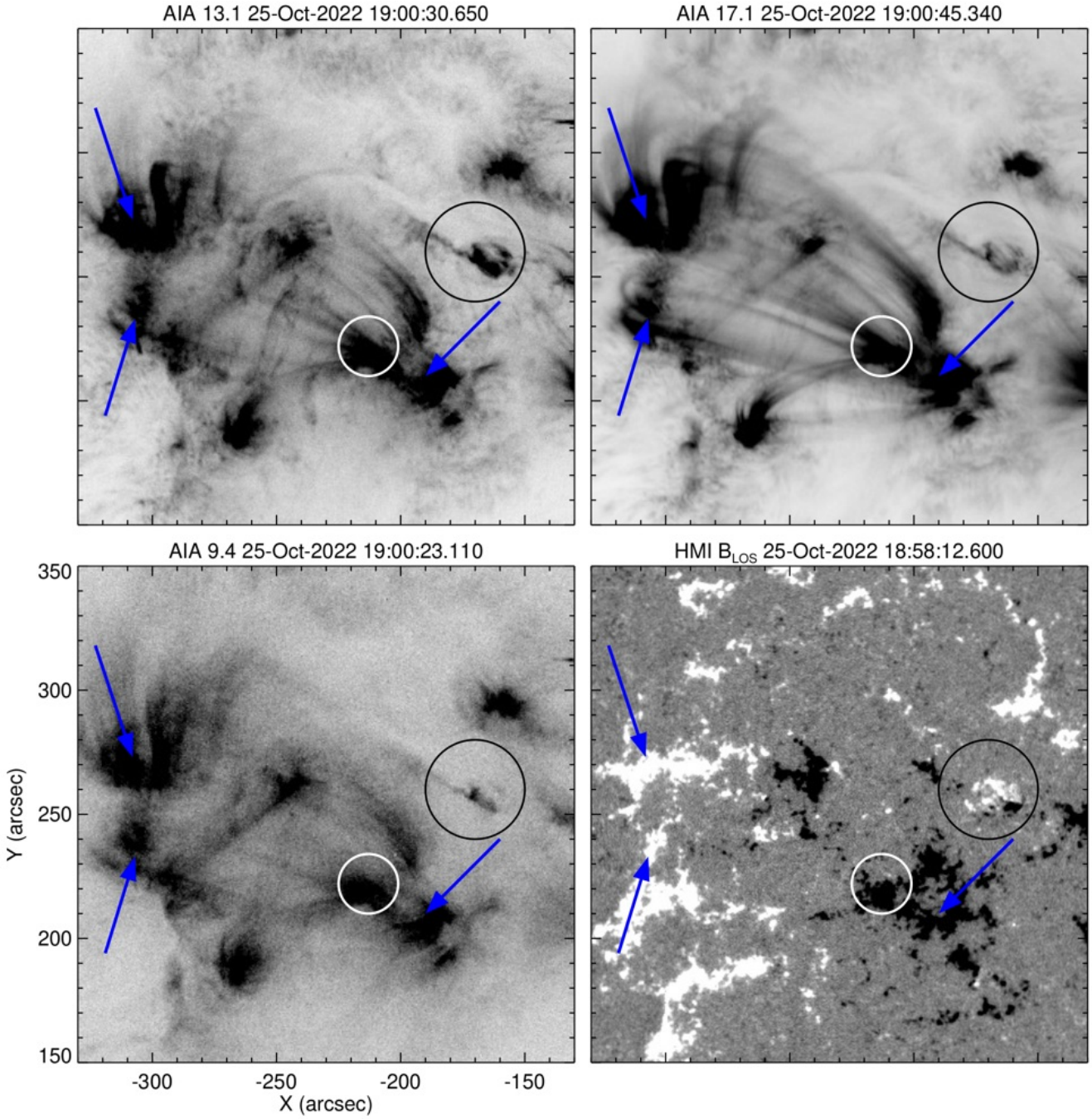

Figure 5. Four images observed from SDO, including the 13.1, 17.1 nm and 9.4 nm AIA images which sample plasmas near 0.5, 1 and 6 MK respectively, outside of flares. Arrows point to locations where the loop system discussed in the text are anchored. The close-up views in Figure 1 are centered near $X = -180, Y = 250$ in this figure. The encircled region in black shows a magnetic bipole emerging during the observations reported here.

is a vast literature on the role of reconnection following a cascade of turbulent motions to unobservable scales (Appendix D of Schekochihin 2022). This second kind of reconnection may well be present, but it is the result of a different primary process, occurring on small scales, and its observational signatures may be hidden below our ability to measure.

To proceed, in the kind of loops observed by EUI, some typical conditions can be estimated from many previous studies (e.g. Jordan 1992). The Alfvén speed is estimated to be

$$c_{\rm A} = \frac{B}{\sqrt{4\pi\rho}} \approx 2800\ \frac{B_{100}}{\sqrt{n_{9.7}}}\ \ {\rm km\ s^{-1}} \qquad (1)$$

where $B_{100} \sim 1$ is the magnetic field strength in units of 100 G, and $n_{9.7} \sim 1$ is the number density of coronal ions in units of $5 \cdot 10^9$ particles per cm^3.

Magnetic reconnection is first and foremost a mechanism for a magnetoplasma system to relax rapidly to a lower energy state via a change in magnetic topology. In doing so, newly unbalanced Lorentz forces accelerate plasma to drive bulk plasma motions to form the exhaust of a small-scale magnetic diffusion region. Other *observed* effects of reconnection as witnessed during flares and plasmoid ejections include particle acceleration, hard X-ray emission and plasma turbulence (e.g. Fletcher et al. 2011). It can be a source of high-frequency waves with additional consequences (Kasper et al. 2013). But these are secondary effects in the highly conducting, large low$-\beta$ corona. They may or may not play an active role in heating the corona.

The speed with which the bulk plasma is swept up by reconnection approaches the Alfvén speed associated with the reconnected vector component of the total magnetic field, $\mathbf{B}_\perp$, where the component along the loop diection is $\mathbf{B}_\parallel$,

$$\mathbf{B} = \mathbf{B}_\parallel + \mathbf{B}_\perp.$$

The weakly varying intensity data from EUI, and subsonic linewidths, would seem to confine the possible role of magnetic reconnection to $\mathbf{B}_\perp$, with $\mathbf{B}_\parallel$ playing just a passive role, as follows. With $\xi \lesssim 30$ km s^{-1} as an estimate of the Alfvén speed of the components of reconnecting magnetic fields, $\mathbf{B}_\perp$, then we can estimate that

$$B_\perp \lesssim\ \xi_{30}\ \sqrt{n_{9.7}}, \qquad (2)$$

where ξ_{30} measures the linewidths in units of 30 km s^{-1}. Thus, if these motions are caused by annihilation of $\mathbf{B}_\perp$, then its magnitude is ≈ 1 G, 1% of the magnetic field strength B expected under typical conditions (e.g. Jordan 1992), also noting the photospheric field strengths of Figure 5. In the "nanoflare" picture of Parker (1988), ratio $B_\perp/B$ equals the angle between magnetic fields separated by tangential discontinuities. Parker (1988) estimated a much larger angle of 0.25 radians. This factor of 25 discrepancy will be explored below.

Further implications from the EUI data on reconnection are debatable, because imaging, even at "small" scales of 150 km, is unable to measure scales at which dissipation must occur, except for a possible role for ion viscous dissipation near 10^2 km (Hollweg 1986; Davila 1987). Undaunted by this, we follow arguments using decades of observations of EUV observations (reviewed by Bogachev et al. 2020), and explore quantitatively what the findings from EUI imply in terms of elementary units (i.e. "quanta") of energy dissipation.

Let us assume that all the brightness variations observed are due to reconnection somewhere within a plasma loop, then Figures 3 and 4 indicate that the majority of pixels within loops have $\sigma_{\rm I}/I_{\rm mean}$ of order 0.01 (see the lower left panel of Figure 3), with occasional fractions rising to 0.25 near specific footpoints. Assume further that each such pixel is connected by rapid heat conduction along the length L of the bundle of flux, so that the 1% variations apply to the entire volume

$$v \approx Lp^2 \qquad (3)$$

where $p = 150$ km is the EUI pixel size. Within volume v let $\mathcal{E}$ erg be the energy released in each reconnection event. The total rate of energy release within volume v is

$$\dot{n}\,\mathcal{E}\ \ {\rm erg\ s^{-1}} \qquad (4)$$

or a volumetric heating rate of

$$\frac{\dot{n}\,\mathcal{E}}{v}\ \ {\rm erg\ cm^{-3}s^{-1}}. \qquad (5)$$

Here, $\dot{n}$ is the number of events of energy $\mathcal{E}$ per unit time. Our immediate aim is to find values of $\mathcal{E}$ and $\dot{n}$ from the statistical variations in the EUI data of loops, using known energy flux density requirements. From previous observations (Withbroe & Noyes 1977), we know that for a loop of length L, the energy flux densities $W_{\rm obs} = 10^7$ erg cm^{-2}s^{-1}, so that

$$\frac{\dot{n}\,\mathcal{E}}{v} \approx \frac{W_{\rm obs}}{L}\ \ {\rm erg\ cm^{-3}s^{-1}},\ \text{and} \qquad (6)$$

$$\mathcal{E} = \frac{W_{\rm obs}p^2}{\dot{n}}\ \ {\rm erg}. \qquad (7)$$

To estimate $\dot{n}$, we use the EUI observation that $\sigma_{\rm I} \sim 0.01 I_{\rm mean}$, for the bulk of the loop system seen in the figures. When $I_{\rm mean}$ and $\sigma_{\rm I}$ result from statistical fluctuations of n quanta of energy, then $1/\sqrt{n} \sim \sigma_{\rm I}/I_{\rm mean}$. Then $n \sim (I_{\rm mean}/\sigma_{\rm I})^2$. For variations of 0.01, we find

$\dot{n} \approx 10^4/1800$ quanta per second, from which

$$\mathcal{E} \approx 4 \cdot 10^{20} \text{ erg}, \tag{8}$$

three to four orders of magnitude smaller than Parker's original 1988 estimate. Note that $\mathcal{E}$ varies as the area of each instrument's pixel. If larger variations of order 0.1 are present in, say, the 28.4 nm band, then $\dot{n} \sim 100/1800$ quanta per second, 100 times smaller, and the energy in each event would be $\mathcal{E} \approx 4 \cdot 10^{22}$ erg.

Alternatively if $\mathcal{E}$ were instead 10^{24} erg (a "nano-flare", Parker 1988), we would expect to see changes of order unity along the loops in the EUI images. Or, for a pixel size of say $p = 725$ km (1″ from Earth's orbit), the rms variations would be reduced by the factor $725/150 \approx 5$. For the 725 km pixels, fractional brightness variations would be reduced to 0.2.

The far smaller estimate of the energy of quanta given by equation (8) results from both the small pixel areas p^2 available from the EUI on Solar Orbiter, as well as the tiny 1-2% rms changes of intensity measured along these loops. Of course, these results explicitly assume energy released in quanta, and they must be upper limits because other sources of brightness variations, such as waves, flows, have been ignored. Next we try to reconcile the divergence of the present results from those found earlier.

4.3. *Nanoflares revisited*

Parker's 1988 estimate of the properties of nano-flares with energies of order 10^{24} erg was originally derived using two sources of data:

1. The average energy loss of the active coronal plasma is $W_{\rm obs} = 10^7$ erg cm^{-2} s^{-1} from Withbroe & Noyes (1977).

2. This is supplied by work done by convectively-driven photospheric plasma on magnetic fields emerging upwards into the active corona. He adopted thermodynamic parameters from observations of granules, lifetimes τ of 500 seconds and horizontal (random) velocities of $u = 0.5$ km s^{-1}.

4.3.1. *Parker's original formulation*

The work W per unit time done by horizontal granular motions moving vertical magnetic fibrils of field strength B at a speed u against the magnetic tension force is:

$$W \approx \frac{B_\perp B}{4\pi} u \quad \text{erg cm}^{-2} \text{ s}^{-1}. \tag{9}$$

Assuming from the ideal induction equation that

$$B_\perp \approx B \tan\theta = B \frac{ut}{L}, \tag{10}$$

where θ is the average angle between magnetic field vectors on either side of a tangential discontinuity, then

$$W \approx \frac{(uB)^2}{4\pi L}\, t \quad \text{erg cm}^{-2} \text{ s}^{-1}. \tag{11}$$

With $B = 100$ G, and for a loop of length $L = 100$ Mm, the time needed to generate $W_{\rm obs}$ is $t = T \sim 5 \cdot 10^4$ seconds $\approx 100\tau$, $\theta \approx 0.25$ radians, the total footpoint displacement $uT \approx 25$ Mm, and $B_\perp \sim 0.25B$. The total footpoint displacement must occur through the addition of $m \approx 100$ increments of length $u\tau$. For each increment the energy released by reconnection across the current sheet is

$$\mathcal{E} \approx \frac{B_\perp^2}{8\pi} \mathcal{V} \approx 10^{24} \quad \text{erg} \tag{12}$$

where the volume $\mathcal{V} \approx (u\tau)^2 \Delta L$ cm^3, with $\Delta L = L/m \approx 1000$ km is the extension along the coronal loop of each current sheet element. The volume $\mathcal{V}$ is product of the ΔL, $u\tau$ and the width of the flux bundle, also assumed to be $\approx u\tau = 250$ km.

4.3.2. *A revision of Parker's scenario*

Another Parker-like estimate of $\mathcal{E}$ comes from integrating equation (11) in time. Let us assume that energy is released in quanta after time $t = T$ with energy $\mathcal{E}$, and solve for these quantities given Parker's parameters. A random walk with $m > 1$ steps of duration τ, each of length $u\tau < L$, yields

$$B_\perp \approx B \tan\theta = B \frac{\sqrt{m}\, u\tau}{L}, \tag{13}$$

so that in time $T = m\tau$

$$W \approx \frac{(uB)^2}{4\pi L} \sqrt{m}\tau \quad \text{erg cm}^{-2} \text{ s}^{-1}. \tag{14}$$

With $W = W_{\rm obs}$, $\sqrt{m}\tau = T = 5 \cdot 10^4$ seconds as above, we find instead $m \approx 10^4$. The path length over which work is done is $\sqrt{m}u\tau$ instead of Parker's $mu\tau = T$, so that each quantum releases

$$\approx \frac{(uB)^2}{8\pi L} T^2 \quad \text{erg cm}^{-2}, \text{ and so} \tag{15}$$

$$\mathcal{E} \approx \frac{(uB)^2}{8\pi L} \mathcal{A} T^2 \quad \text{erg}. \tag{16}$$

The net area swept out by the moving bundle is $\mathcal{A} \approx mu\tau \cdot \ell$ where ℓ is the characteristic size length of the flux bundle perpendicular to $\mathbf{u}$ and $\mathbf{B}$. Using $\ell \approx u\tau$, then

$$\mathcal{E} \approx 10^{21} \quad \text{erg}, \tag{17}$$

three orders of magnitude smaller than Parker's original estimate.

4.3.3. *Further constraints*

With knowledge of mass densities ρ associated with the observable unresolved motions of amplitude ξ, whether waves or ensembles of reconnection jets, the energy flux W can be estimated through

$$W \lessapprox \rho\,\xi^2\,c \tag{18}$$

with c the group speed of the waves and/or speed of ordered plasma motions in jets. The inequality must be used because the above estimate assumes all energy propagates upwards, and becomes dissipated within coronal plasma along the magnetic flux bundle. Combining the above estimates of ρ, ξ and using $c = c_{\rm A}$, we find

$$W \lessapprox 3\ 10^7 \sqrt{n_{9.7}}\ \xi_{30}^2\ B_{100}. \tag{19}$$

Independent of estimates of energy fluxes from nanoflares, $W_{\rm obs}$ requires line widths ξ of order 30 km s^{-1}.

Observed coronal line widths are $\xi \sim 30$ km s^{-1} (e.g. Del Zanna & Mason 2018), corresponding to $\xi \sim 0.2 c_{\rm S}$ with $c_{\rm S}$ the sound coronal speed. Using as a rough estimate to satisfy the inequality above, $\xi \sim 0.5 c_{\rm S}$, these speeds can be identified with the Alfvén speed of the annihilated component $B_\perp$ in Parker's picture. Then $B_\perp \sim B 0.5 c_{\rm S}/c_{\rm A}$, or $\tan\theta \sim 0.5 c_{\rm S}/c_{\rm A} \sim 0.3\beta$, where the plasma $\beta = 8\pi p/B^2 \sim 0.01$.

Thus we arrive at the independent estimate for the annihilated magnetic component $B_\perp \approx 0.01 B$ using equation (19). This should be contrasted with $B_\perp \approx 0.25 B$ as suggested by Parker.

In summary, it is proposed that Parker's picture, if it is indeed the source of heating of the active corona, be quantitatively modified such that the nano-flares are more pico-flares with energies $\lesssim 10^{21}$ erg. The tangential discontinuities are accordingly weak (misaligment angles of $\sim$ 0.01 radians). Any reconnection of the perpendicular components occurs rapidly at lower alignment angles and electric current densities than derived by Parker. It is quite possible, in the absence of data to the contrary, that processes other than reconnection may cause the apparently steady heating rates inferred from the new EUI data, such as dissipative surface waves (Ionson 1978), dissipation of compressive ion motions (Hollweg 1986; Davila 1987), MHD turbulence (Rappazzo et al. 2007, 2008; Einaudi et al. 2021) and wave dynamics in inhomogeneous conditions (Howson et al. 2020). The 3D numerical MHD experiments of Einaudi et al. (2021), including stratification and treatments of thermodynamics, independently arrived at energies between 10^{18} and 10^{21} erg for their "elementary events". Although MHD may not be applicable across the range of scales leading to irreversible dissipation, in particular at kinetic scales (mean free paths are a few hundred km), Einaudi et al. (2021) argued that the total energies of elementary events is independent of magnetic Reynolds number. The convergence of these two results is interesting.

Lastly, the number of pico-flares per unit area per unit time is

$$\frac{n}{Lpt} \sim 4 \cdot 10^{-17}\ \ {\rm cm}^{-2}\ {\rm s}^{-1}$$

This lies within the errors in the relation $\log_{10} N(E) = 30.6 - (2.18 \pm 0.2) \log_{10} E$, of the form $N(E) \propto E^{-\alpha}$, values derived from SDO data (Ulyanov et al. 2019). When $\alpha > 2$ the heating is dominated by small events. Thus pico-flares, if indeed are responsible for the EUI variability, are a dominant contributor to coronal heating in active regions.

4.4. *Consequences*

On scales down to 150 km, the solar corona observed by EUI at 17.1 nm exhibits essentially two kinds of phenomena. The first dominates almost all of the active corona almost all the time. While not a unique interpretation, the idea of quanta of small flares has been extended to pico-flare scales (10^{21} erg) enabled through the almost unprecedented spatial sampling of $p = 150$ km, the very small variances, and the long time series (1800 seconds) of the EUI observations. Other physical mechanisms than small flaring may prove to be entirely compatible with the EUI data, no attempt to refute them is made here. In one sense, the "nano-flare" picture of Parker remains intact, but at far smaller scales.

The second kind appears to be connected with more explosive behavior which has drawn the attention of decades of solar observers. We have no measurements of magnetic field changes, just changes in image morphology, to support our claim. So at this stage it remains a hypothesis to be tested. But the consequences are pivotal in our quest to understand the solar corona. A host of models for bulk coronal heating based upon reconnection must now be challenged. For example, models by Priest et al. (2002), drawing on the interaction of convection-driven multipolar fields on scales of Mm and above must be called into question. This particular model, as well as all models based on multipolar magnetic fields (Dowdy et al. 1986; Antiochos & Noci 1986; Hansteen et al. 2014) also fails to capture elementary properties of the hot plasmas in relation to chromospheric magnetic fields measured recently with DKIST (Judge et al. 2023).

Lastly, we note that the well-studied phenomenon of coronal rain, sensitive to excess heating events, fills less than about 3% of the active corona by volume (Antolin

et al. 2015). This might suggest, again, that the bulk of the time the corona is in a state where excessive heating events are rare, and the corona appears to be steadily heated on very small scales for long periods of time (1800 seconds), longer than loop cooling times.

4.5. *Conflicts with earlier work?*

These results appear to be in direct conflict with much earlier work, yet arguably they are based upon the most stable set of coronal data ever obtained, at the highest angular resolution. These data are also compatible with the decades-long set of measurements of unresolved motions in the "undisturbed" corona. Here, an attempt to explain this discrepancy is made through examining the methods used elsewhere which have delivered a different kind of understanding.

Firstly, Parker's (1988) article on nanoflare heating was prompted by full-Sun observations of hard X-rays by Lin et al. (1984). The X-ray data on 27 June 1980 were from a day close to the sunspot maximum with at least 15 intense bipolar regions on the disk, as judged from the Kitt Peak Vacuum Telescope magnetograms acquired around 18:00 UT (as stored in the Virtual Solar Observatory archive). Lin et al. found that hard X-ray bursts ($>$ 20 keV) occurred about one every 5 minutes above a flux of $\sim 7\ 10^3$ cm^{-1} s^{-1} keV^{-1}). They speculated that the energy of the accelerated electrons might be comparable to that required to heat the active corona. However, no sources were identified on the Sun in these full-Sun measurements. The relation of this early work to the data presented here are at best, questionable. There is clearly no direct conflict between these two sets of data.

A second tentative conflict arises considering observations of transition-region plasma (here we use a definition to include all plasma emitting from the Sun between electron temperatures of 20,000 and 500,000 K) from high resolution instruments beginning in 1975 have been widely interpreted to be highly dynamic (see the review by de Pontieu et al. 2021). Given that at least some transition region emission must originate from electron heat conduction down from the corona, this has led to the expectation that the corona itself must be dynamic, even in the quiet Sun. The impression is that the problem of coronal heating is one of a highly dynamic system driven by photospheric motions (subsonic motions with time scales of minutes), involving many kinds of instabilities and/or flares (e.g. Pontin & Priest 2022; Raouafi et al. 2023, and many references in these works). Again, any conflict between the EUI data analyzed here and transition region dynamics inferred in multiple earlier studies is at best, indirect. In particular we note that coronal emission lines rarely show the signatures in Doppler shifted transition region lines of order 100 km s^{-1}, even though coronal plasma appears to be more tenuous and should reflect such dynamics. The transition region also has its own basic challenges. The entire mass of the emitting plasmas is so small that modest changes in energy from chromosphere or corona can dominate the dynamics.

Thirdly, much of the reported evidence for dynamics is only *indirect*, often depending on a series of multiple assumptions untested or currently untestable. For example, the review of Viall et al. (2021) includes discussions of multi-thread, nano-flare driven, and other empirical constructs in order to account for apparent contradictions of data with *ad-hoc* models within the standard paradigm. Should we to accept "over-density" of loops as strong evidence for dynamics, and if so, on what length- and time-scales? Without delving deeper into multiple underlying assumptions in these earlier studies, it seems best to draw attention to the non-uniqueness of data interpretations under the usual paradigm, the limitations of remote sensing, and acknowledge that frequently used theories (such as fluid mechanics) have no solid prior justification. Indeed, others have proposed yet-to-be-refuted solutions using assumptions far outside of these models (e.g. Scudder 1992)).

Lastly, in a paper entitled "Dominance of Bursty over Steady Heating of the 4-8 MK Coronal Plasma in a Solar Active Region: Quantification Using Maps of Minimum, Maximum,and Average Brightness" Tiwari et al. (2023) studied the same kind of question with very different results. We might speculate that perhaps the results apply to the far hotter plasmas observed at 9.4 nm in emission from Fe XVIII ions formed near 4-8 MK. But other differences in methods (power spectra versus reproducible but subjective measures of variability on longer time scales), lower sampling in space and time, make meaningful comparisons difficult. It would be interesting to pursue both kinds of data using the same techniques and data sampling rates.

The arguments presented here contend that the EUI data here are sufficient in themselves to prompt new future lines of inquiry, perhaps outside of the usual set of underlying assumptions.

5. FUTURE WORK

Beyond these straightforward observations, little quantitative can be said. Future analysis should include a feature identification algorithm, which also "knows" about the amplitudes of variations in time shown in the figures in this paper. Machine learning techniques agnostic to objects under study would appear to offer a

natural way forward. For example, the analysis would benefit from identifying what are reasonably identifiable as transverse oscillations and/or field-aligned flows in the time series, whose only irreversible processes might include radiation losses, but no heating *per se*. Then, at least, such features could arguably be ruled out of the more interesting cases where magnetic morphology, and perhaps topology, is changing. Such feature classification would also provide confidence in assigning the statistical samples to specific kinds of structure, hopefully to provide more precise estimates of properties required by pico-flares and other mechanisms which remain as yet unrefuted, in particular near loop footpoints where brightness variations are often, but not always, larger than 1%.

One more revision of Parker's analysis might also be considered. Unresolved chromospheric motions, spectroscopic "turbulence", exceed those of the photosphere by roughly an order of magnitude (e.g. Athay 1976; Vernazza et al. 1981; Judge et al. 2020). But it is unclear yet upon what scale these motions occur and if they have cross-field components to generate $B_\perp$ to produce the needed work rate W. If so, and they exist on large enough scales ($> u\tau$), then again with $B \approx 100$ G at the top of the chromosphere (this was essentially assumed by Parker at the coronal base), $u \approx 5$ km s^{-1}, $T \approx 500$ seconds. Then $m = 1$, $\tan\theta \approx 0.025$ radians, $B_\perp = 2.5$ G, and $\mathcal{E} \approx 10^{23}$ erg. This consideration points to the need for a better understanding of the dynamics of plasma across the magnetic fields in the upper chromosphere, using DKIST and other large solar telescopes.

The agreement between the analysis from Solar Orbiter EUI data and the numerical experiments of Einaudi et al. (2021) should be explored further. It will be interesting to see how future developments in computing and observations, confronted in the manner presented here, might limit the range of coronal heating mechanisms

Similar datasets from the EUI might also be examined, especially given the recent broad interest in the origins of dynamic magnetic fields measured by the Parker Solar Probe near $10R_\odot$. On the basis of the present paper, these would seem to arise only through events related to the emergence of magnetic flux and accompanying rapid magnetic changes (Raouafi et al. 2023).

ACKNOWLEDGMENTS

The author is grateful to the International Space Science Institute for a visiting fellowship in February 2023 where he was introduced to the Solar Orbiter data. He thanks Lucia Kleint and the astronomy department at the University of Bern and the Swiss National Science Foundation (grant No. 216870) which made this work possible. Alin Paraschiv is gratefully acknowledged for comments on the script. This material is based upon work supported by the National Center for Atmospheric Research, which is a major facility sponsored by the National Science Foundation under Cooperative Agreement No. 1852977.

REFERENCES

Alfvén, H. 1942, Nat., 150, 405

Antiochos, S. K., & Noci, G. 1986, ApJ, 301, 440

Antolin, P., Vissers, G., Pereira, T. M. D., Rouppe van der Voort, L., & Scullion, E. 2015, ApJ, 806, 81, doi: 10.1088/0004-637X/806/1/81

Aschwanden, M. J. 2001, ApJ, 560, 1035, doi: 10.1086/323064

Athay, R. G. 1976, The Solar Chromosphere and Corona: Quiet Sun (Dordrecht: Reidel)

Auchère, F., Soubrié, E., Pelouze, G., & Buchlin, É. 2023, A&A, 670, A66, doi: 10.1051/0004-6361/202245345

Billings, D. 1965, The Solar Spectrum - the Coronal Spectrum. (D. Reidel Publ. Co.)

Bogachev, S. A., Ulyanov, A. S., Kirichenko, A. S., Loboda, I. P., & Reva, A. A. 2020, Physics Uspekhi, 63, 783, doi: 10.3367/UFNe.2019.06.038769

Bray, R. J., Loughhead, R. E., & Durrant, C. J. 1984, The Solar Granulation (Cambridge UK: Cambridge Univ. Press)

Brooks, D. H., & Warren, H. P. 2016, ApJ, 820, 63, doi: 10.3847/0004-637X/820/1/63

Coyner, A. J., & Davila, J. M. 2011, ApJ, 742, 115, doi: 10.1088/0004-637X/742/2/115

Davila, J. M. 1987, ApJ, 317, 514

Davila, J. M. 1994, ApJ, 423, 871

De Moortel, I., & Browning, P. 2015, Philosophical Transactions of the Royal Society of London Series A, 373, 20140269, doi: 10.1098/rsta.2014.0269

de Pontieu, B., McIntosh, S. W., Hansteen, V. H., & Schrijver, C. J. 2009, ApJL, 701, L1, doi: 10.1088/0004-637X/701/1/L1

de Pontieu, B., Polito, V., Hansteen, V., et al. 2021, Sol. Phys., 296, 84

Del Zanna, G., & Mason, H. E. 2018, Living Reviews in Solar Physics, 15, 5, doi: 10.1007/s41116-018-0015-3
Dowdy, J. F., J., Rabin, D., & Moore, R. L. 1986, Sol. Phys., 105, 35
Einaudi, G., Dahlburg, R. B., Ugarte-Urra, I., et al. 2021, ApJ, 910, 84
Fisher, G. H., Longcope, D. W., Metcalf, T. R., & Pevtsov, A. A. 1998, ApJ, 508, 885
Fletcher, L., Dennis, B. R., Hudson, H. S., et al. 2011, SSR, 159, 19
Hansteen, V., de Pontieu, B., Carlsson, M., et al. 2014, Science, 346, 1255757
Hara, H., & Ichimoto, K. 1999, ApJ, 513, 969
Hollweg, J. V. 1986, ApJ, 306, 730
Howson, T. A., de Moortel, I., & Reid, J. 2020, A&A, 636, A40
Ionson, J. A. 1978, ApJ, 226, 650
Jordan, C. 1992, Memorie della Societa Astronomica Italiana, 63, 605
Judge, P., Kleint, L., Casini, R., & de Wijn, A. 2023, in preparation
Judge, P. G., & Ionson, J. A. 2023, The Problem of Coronal Heating. A Rosetta Stone for Electrodynamic Coupling in Cosmic Plasma (Springer, in press)
Judge, P. G., Kleint, L., Leenaarts, J., Sukhorukov, A. V., & Vial, J.-C. 2020, ApJ, 901, 32
Kasper, J. C., Maruca, B. A., Stevens, M. L., & Zaslavsky, A. 2013, Phys. Rev. Let, 110, 091102, doi: 10.1103/PhysRevLett.110.091102
Kosugi, T., Matsuzaki, K., Sakao, T., et al. 2007, Sol. Phys., 243, 3
Koutchmy, S., Baudin, F., Abdi, S., Golub, L., & Sèvre, F. 2019, A&A, 632, A86, doi: 10.1051/0004-6361/201935681
Krishna Prasad, S., Singh, J., & Banerjee, D. 2013, Sol. Phys, 282, 427, doi: 10.1007/s11207-012-0160-010.48550/arXiv.1210.6434
Lin, R. P., Schwartz, R. A., Kane, S. R., Pelling, R. M., & Hurley, K. C. 1984, ApJ, 283, 421, doi: 10.1086/162321
Low, B. C. 2023, Physics of Plasmas, 30, 012903, doi: 10.1063/5.0124164
Mandrini, C. H., Démoulin, P., & Klimchuk, J. A. 2000, ApJ, 530, 999
Marsch, E., Marsden, R., Harrison, R., Wimmer-Schweingruber, R., & Fleck, B. 2005, Advances in Space Research, 36, 1360
Marsden, R. G., Müller, D., & StCyr, O. C. 2013, in American Institute of Physics Conference Series, Vol. 1539, Solar Wind 13, ed. G. P. e. a. Zank, 448–453
Norton, A. A., Jones, E. H., Linton, M. G., & Leake, J. E. 2017, ApJ, 842, 3, doi: 10.3847/1538-4357/aa7052
Paraschiv, A. R., & Donea, A. 2019, ApJ, 873, 110, doi: 10.3847/1538-4357/ab04a6
Parker, E. N. 1988, ApJ, 330, 474
Peres, G. 2000, Sol. Phys., 193, 33, doi: 10.1023/A:1005220318987
Pontin, D. I., & Priest, E. R. 2022, Living Reviews in Solar Physics, 19, 1
Priest, E. R., Heyvaerts, J. F., & Title, A. M. 2002, ApJ, 576, 533
Rachmeler, L. A., Bueno, J. T., McKenzie, D. E., et al. 2022, ApJ, 936, 67, doi: 10.3847/1538-4357/ac83b8
Raju, K. P., Sakurai, T., & Ichimoto, K. 2001, in Recent Insights into the Physics of the Sun and Heliosphere: Highlights from SOHO and other Space Missions, ed. P. Brekke, B. Fleck, & J. B. Gurman, Vol. **203**, 488
Raouafi, N. E., Stenborg, G., Seaton, D. B., et al. 2023, ApJ, 945, 28, doi: 10.3847/1538-4357/acaf6c
Rappazzo, A. F., Velli, M., Einaudi, G., & Dahlburg, R. B. 2007, ApJL, 657, L47, doi: 10.1086/512975
—. 2008, ApJ, 677, 1348, doi: 10.1086/528786
Rochus, P., Auchère, F., Berghmans, D., et al. 2020, A&A, 642, A8, doi: 10.1051/0004-6361/201936663
—. 2022, A&A, 665, C1, doi: 10.1051/0004-6361/201936663e
Rosner, R., Tucker, W. H., & Vaiana, G. S. 1978, ApJ, 220, 643
Schekochihin, A. A. 2022, Journal of Plasma Physics, 88, 155880501, doi: 10.1017/S0022377822000721
Schmelz, J. T., & Winebarger, A. R. 2015, Philosophical Transactions of the Royal Society A: Mathematical, Physical and Engineering Sciences, 373, 20140257, doi: 10.1098/rsta.2014.0257
Schrijver, C. J., de Rosa, M. L., Title, A. M., & Metcalf, T. R. 2005, ApJ, 628, 501, doi: 10.1086/430733
Scudder, J. D. 1992, ApJ, 398, 299
Singh, J., Sakurai, T., Ichimoto, K., Suematsu, Y., & Takeda, A. 2002, PASJ, 54, 793, doi: 10.1093/pasj/54.5.793
Sturrock, P. A. 1999, ApJ, 521, 451, doi: 10.1086/307544
Thomas, R. J., & Neupert, W. 1994, ApJS, 91, 461
Tiwari, S. K., Wilkerson, L. A., Panesar, N. K., Moore, R. L., & Winebarger, A. R. 2023, ApJ, 942, 2, doi: 10.3847/1538-4357/aca541
Tsuneta, S. 1996, in NATO Advanced Study Institute (ASI) Series C, Vol. 481, Solar and Astrophysical Magnetohydrodynamic Flows, ed. K. C. Tsinganos & A. Ferrari, 85–108
Ulyanov, A. S., Bogachev, S. A., Reva, A. A., Kirichenko, A. S., & Loboda, I. P. 2019, Astronomy Letters, 45, 248, doi: 10.1134/S1063773719040078

Vernazza, J., Avrett, E., & Loeser, R. 1981, ApJS, 45, 635

Viall, N. M., De Moortel, I., Downs, C., et al. 2021, in Solar Physics and Solar Wind, ed. N. E. Raouafi & A. Vourlidas, Vol. 1, 35, doi: 10.1002/9781119815600.ch2

Wiegelmann, T., & Sakurai, T. 2021, Living Reviews in Solar Physics, 18, 1, doi: 10.1007/s41116-020-00027-4

Withbroe, G. L., & Noyes, R. W. 1977, Ann. Rev. Astr. Astrophys., 15, 363